Journal of Geophysical Research: Earth Surface

Supporting Information for

Uncertainties in Shoreline Projections to 2100 at Truc Vert beach (France): Role of Sea-Level Rise and Equilibrium Model Assumptions

M. D'Anna[1,2], B. Castelle[2], D. Idier[1], J. Rohmer[1], G. Le Cozannet[1], R. Thieblemont[1],

and L. Bricheno[3]

[1]BRGM, French Geological Survey, Orléans, France.

[2]Université de Bordeaux, UMR EPOC, CNRS, Pessac, France.

[3]National Oceanography Center, Liverpool, UK.

Contents of this file

Introduction

The present supporting material provides a detailed description of: the method adopted for wave projections correction; the assessment of model free parameters probability distributions; and the results of the test application (outlined in Section 5.3 of the main text) for the *ShoreFor* model.

Text S1. Wave projections correction

The future wave projections issued by Bricheno and Wolf (2018) (hereafter BW18) are the product of a wave model forced with one downscaled Global Climate Model (GCM) outputs. Therefore, the wave projections inherit systematic errors associated with simplified representation of physical processes in the GCM, and/or numerical parametrization within the GCM and the wave model. We perform a seasonal *quantile-quantile* (q-q) comparison between the NORGAS-UG and BW18 wave *historic* time series over the period 1994-2004, and derive a coefficient for each quantile to reduce biases in the BW18 modelled time series. For each season, we compare 101 quantiles (from 1st to 99th with 1% step, plus 0.5th and 99.5th) of H_s, T_p and D_m (Figure S1), and we estimate correction coefficients as follows:

$$C_X{}^{qi} = X_N{}^{qi} - X_{BW}{}^{qi} \quad (S1)$$

Where X is the analysed variable (H_s, T_p or D_m), qi is the i-th quantile, and C is the corresponding correction coefficient. N and BW indicate the NORGAS-UG (reference) and BW18 (to correct) datasets, respectively. At each time step, the values of BW18 H_s, T_p and D_m are corrected using the coefficient corresponding to the nearest quantile of the variable:

$$X^*{}_{BW}{}^{qi} = X_{BW}{}^{qi} + C_X{}^{qi} \quad (S2)$$

Where $X^*{}_{BW}$ is the corrected BW18 variable. The q-q plot of corrected seasonal BW18 time series are shown in Figure S2.

Text S2. Model free parameters probability distribution

In the present work, we determined the joined probability distribution of model parameters by fitting an empirical multivariate distribution on an ensemble of model parameters combinations that produced sufficient model skill against observed shoreline data.

We determined the shoreline change models' performance using the Nash-Sutcliffe (Nash and Sutcliffe, 1970) efficiency score (*NS*), calculated as follows:

$$NS = 1 - \frac{\sum_{n=1}^{N}(Y_m{}^n - Y_o{}^n)^2}{\sum_{n=1}^{N}(\bar{Y_o} - Y_o{}^n)^2} \quad (S3)$$

where N is the number of observations, $Y_m{}^n$ and $Y_o{}^n$ are the n-th modelled and observed shoreline positions, respectively, and $\bar{Y_o}$ is the mean of the observed shoreline positions. The maximum *NS*s

obtained using the optimized model parameters are 0.63 and 0.83 step for SF and Y09, respectively. For the two shoreline models, we investigate different values of the *NS* lower limit (NS_{min}), and we analyse the resulting empirical probability distributions of model parameters with the corresponding behaviour of modelled shoreline. We started by setting NS_{min} to 0.60 and 0.80 for SF and Y09, respectively, then we iteratively reduced NS_{min} with a 0.05 step. We assumed that the NS_{min} decrease is no longer acceptable when this causes abrupt changes in the probability distributions of the model parameters (e.g. emergence of isolated peaks) that associate unrealistic modelled shoreline evolution patterns. For SF, the procedure resulted in an $NS_{min} = 0.25$, with lower values producing a new isolated peak in the parameters distribution (Figure S3) that associated a near-flat modelled shoreline trend. Variations of NS_{min} down to $NS_{min} = 0.25$ did not show abrupt changes to the Y09 parameters distribution, and the modelled shoreline evolution remained realistic. Thus, we assessed the parameter distributions of both shoreline models by selecting the combinations of parameters producing $NS \geq 0.25$.

Text S3. Test application with *ShoreFor*

Here, we analyse the results of the Global Sensitivity Analysis (GSA) on shoreline projections obtained using the SF model in the test application described in Section 5.3 of the main text (i.e. including ensemble wave time series).

The GSA results show that the introduction of uncertainties in the temporal distribution of wave events (Figure S4a) has a large impact on the variance of model results (Figure S4b) and, in turn, on the relative contributions of the remaining uncertain input parameters (Figure S4c-f). However, we note that the wave forcing's *Si* decays rapidly over the last 5 simulated years (Figure S4g) causing the SLR's *Si* to compensate the responsibility to model variance growing rather unnaturally (Figure S4e). This behaviour is likely to be non-physical. Indeed, it is due to the nature of the SF model and the approach used to create the synthetic wave time series. In particular, the SF *r* parameter (Equation S4), which defines the ratio between k_s^+ and k_s^-, is such that the trend in modelled shoreline is conditioned to the trend in wave forcing (Splinter et al., 2014a). Therefore, given that all the synthetic wave time series are constrained by the same long-term trend of the reference BW18 time series, the *r* parameter will tend to reproduce the same trend by the end of the simulated period. The latter results in the tendency of the 3000 modelled shoreline trajectories to converge when approaching the end of the simulation.

$$r = \left| \frac{\sum_{i=1}^{N} \langle F^+ \rangle}{\sum_{i=1}^{N} \langle F^- \rangle} \right| \quad (S4)$$

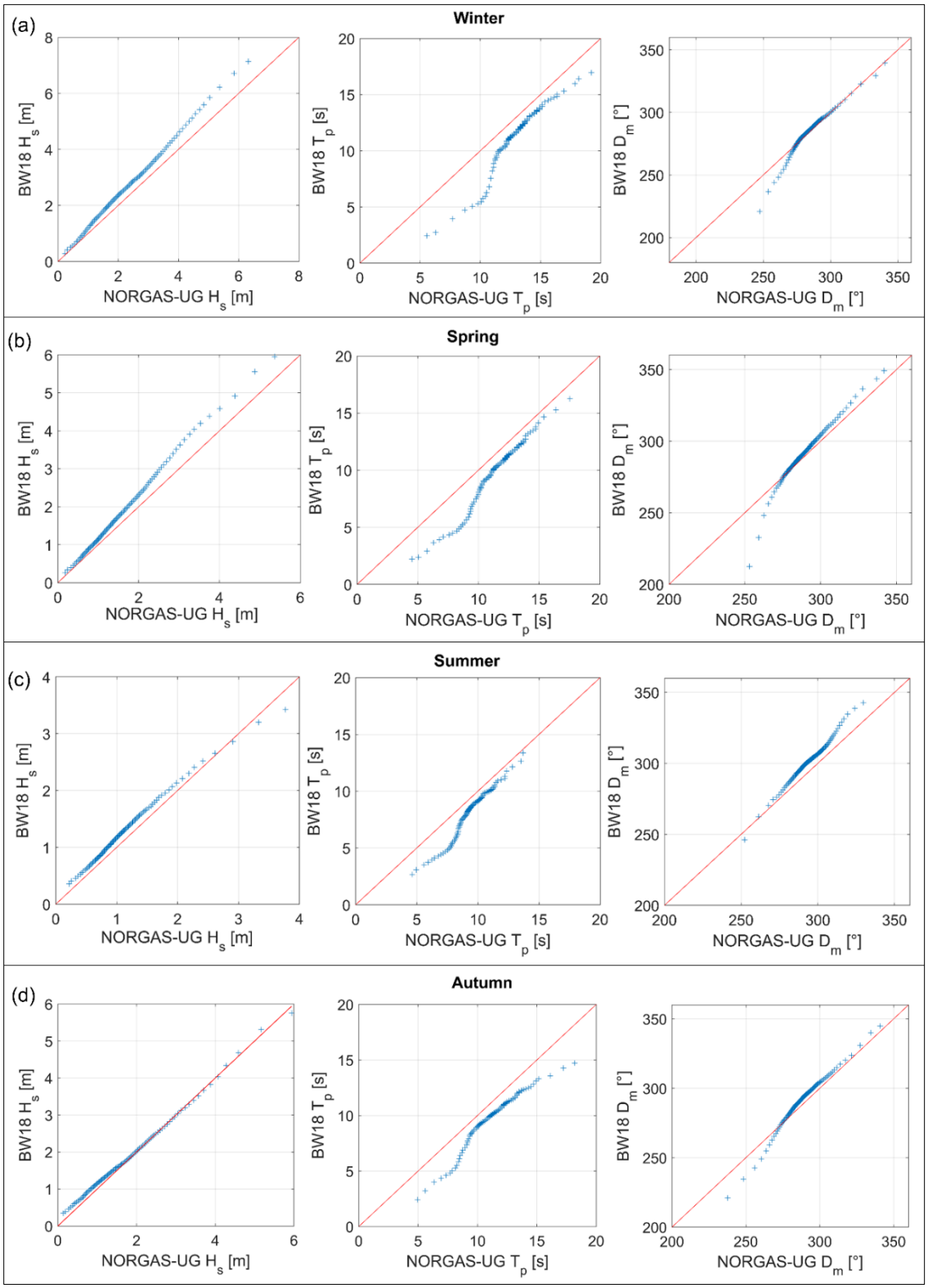

Figure S1 Comparison between NORGAS-UG and Bricheno and Wolf (2018) hindcasts from 2006 to 2020. Quantile-quantile plots of H_s, T_p and D_m time series assessed for (a) winter, (b) spring, (c) summer, and (d) autumn.

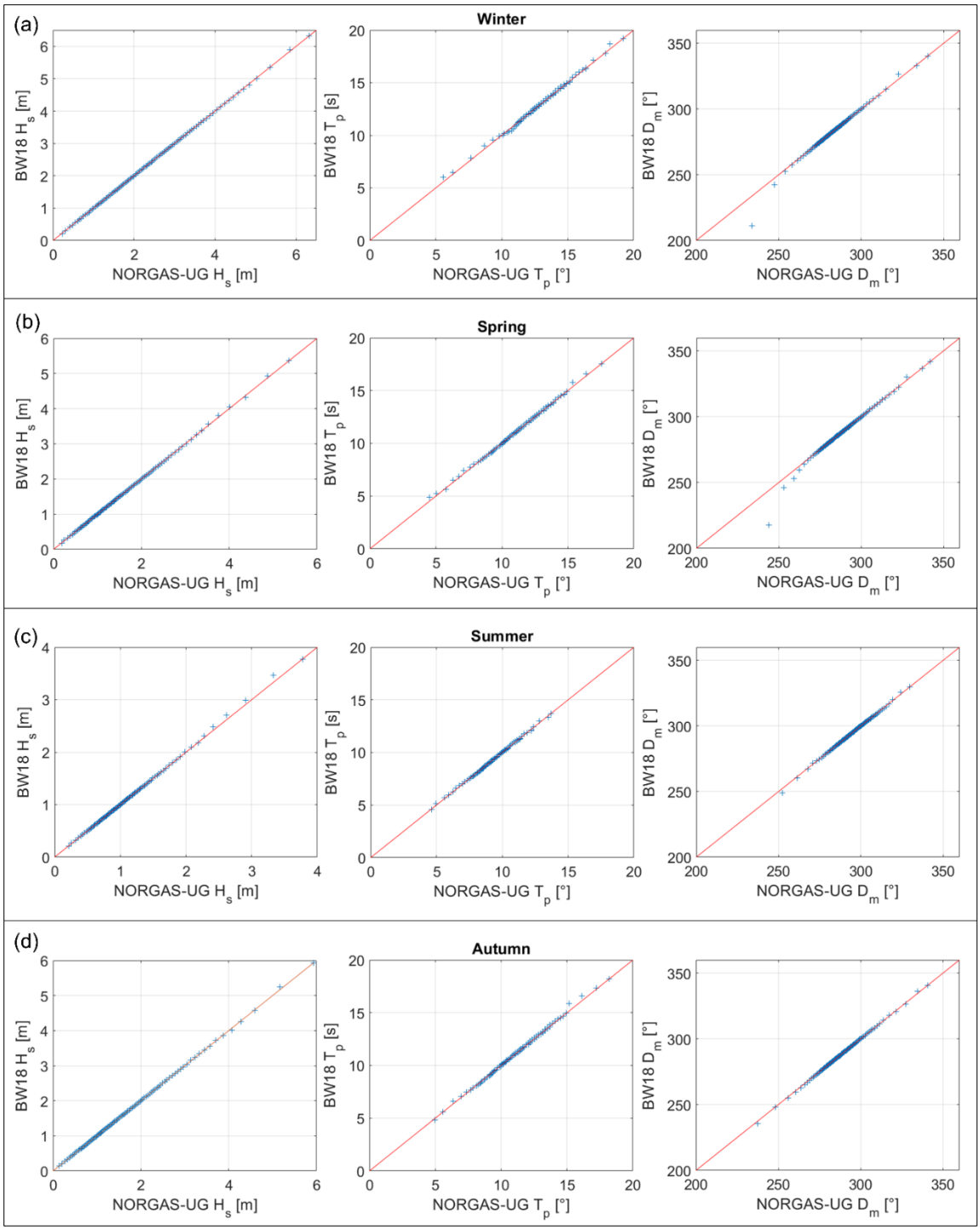

Figure S2 Comparison between NORGAS-UG and the corrected Bricheno and Wolf (2018) hindcasts from 2006 to 2020. Quantile-quantile plots of H_s, T_p and D_m time series assessed for (a) winter, (b) spring, (c) summer, and (d) autumn.

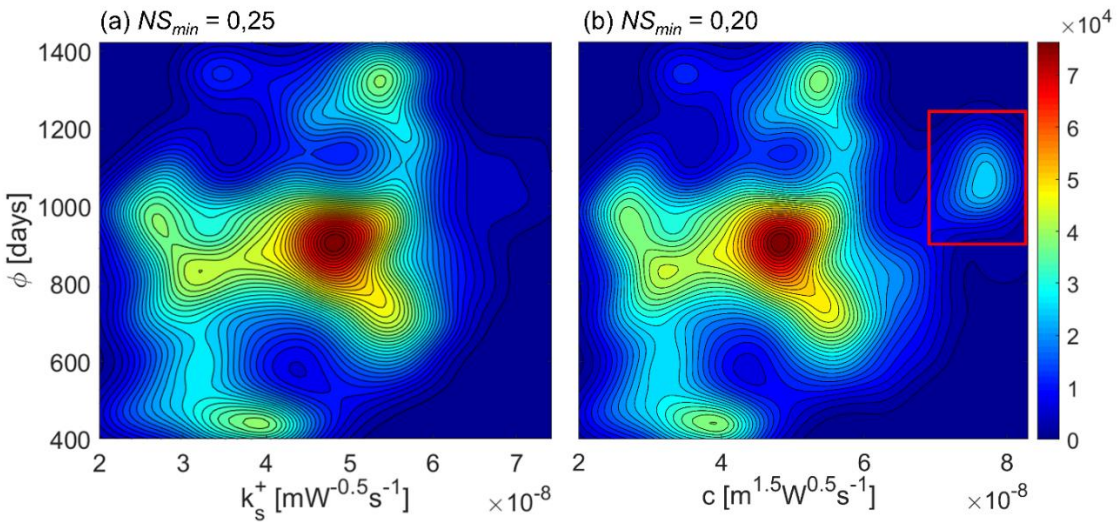

Figure S3 Comparison of *ShoreFor* model parameters probability distributions obtained using combinations of model parameters producing (a) $NS \geq 0.25$, and (b) $NS \geq 0.20$ where a peak emerges (red box).

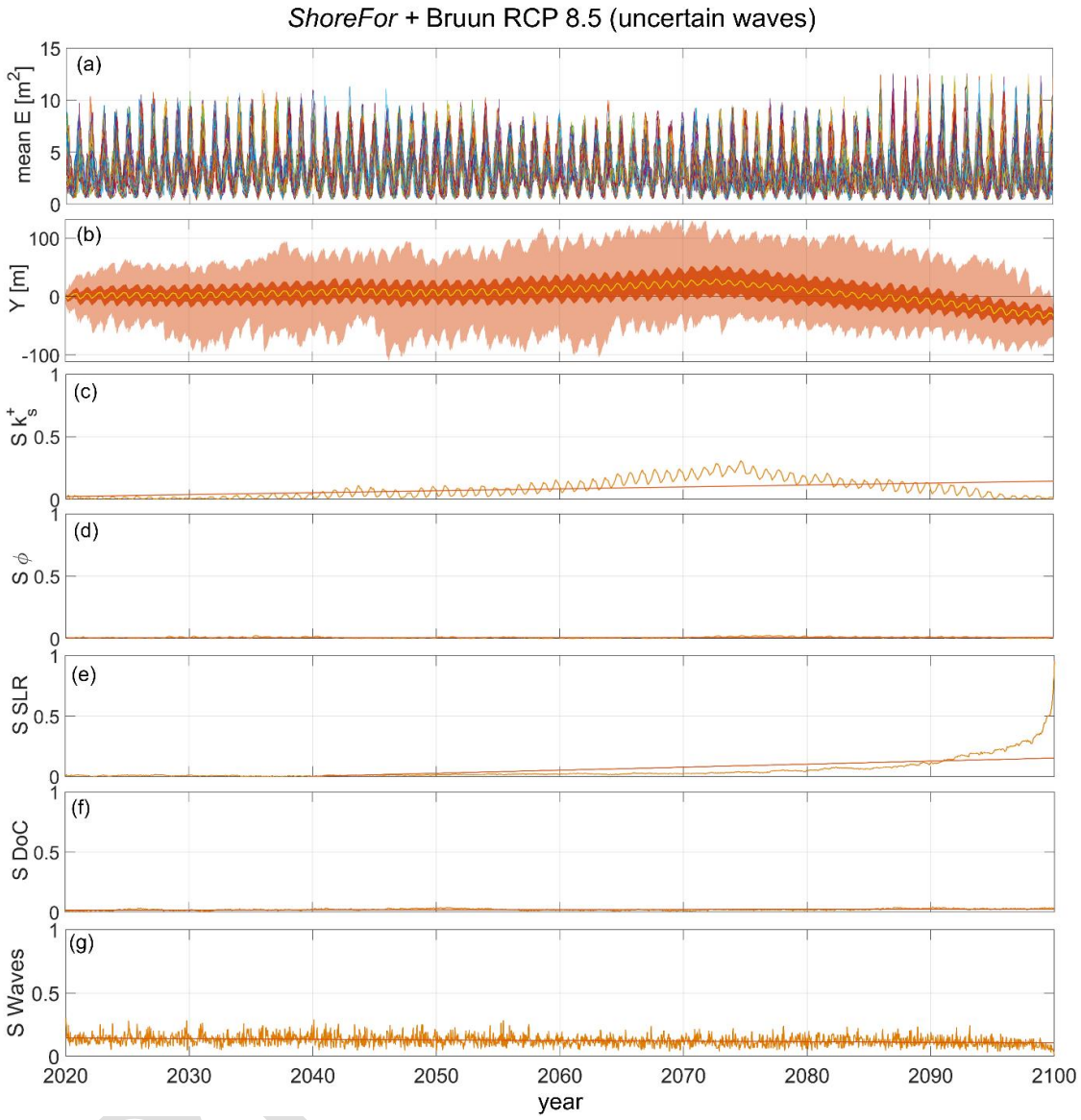

Figure S4 Ensemble of 3000 *ShoreFor* simulations forced using (a) 100 synthetic wave time series from 2020 to 2100 generated with the Davidson et al. (2017) method based on BW18 wave projections for the RCP8.5 scenario; (b) Ensemble shoreline projections over the analysed period; First-order Sobol' index time series for (c) k_s^+, (d) Φ, (e) sea-level rise, (f) depth of closure, and (g) wave energy.

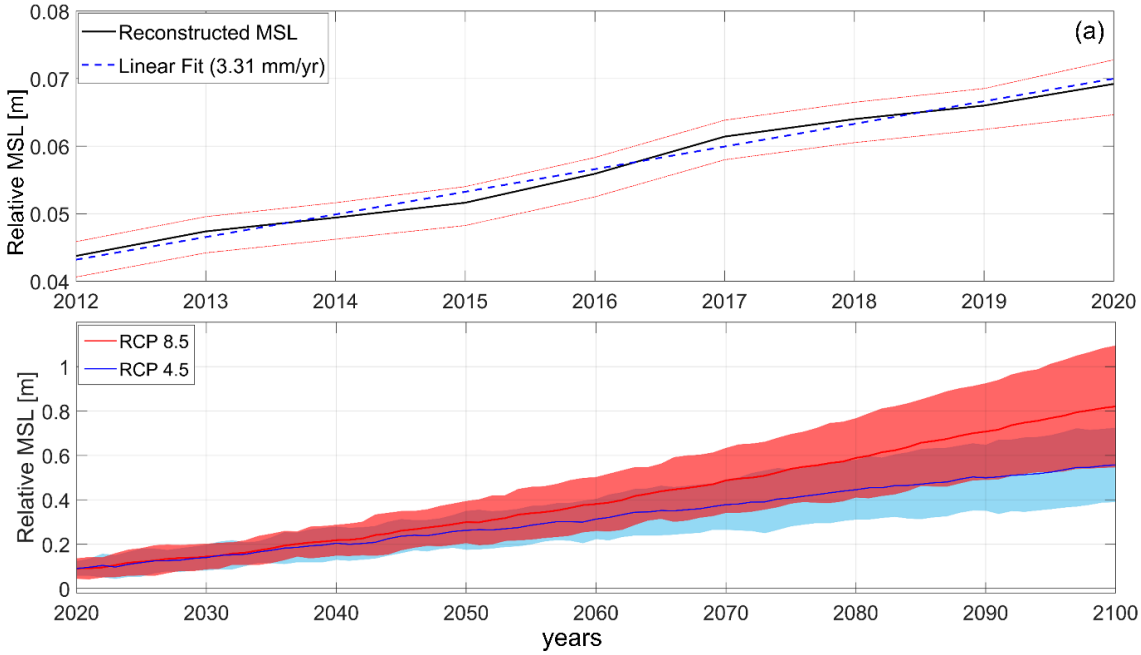

Figure S5 (a) Reconstructed relative mean sea level changes at Cap-Ferret (black line) with standard deviation (red dotted lines) and linear fit (blue dashed line), at the Bay of Biscay over the period 2012-2020; (b) Relative mean sea-level projections from 2020 to 2100 for RCP8.5 (red) and RCP4.5 (blue) scenarios, including 50th percentile (solid lines) and 83% confidence bounds (shaded areas).